

Communication

High-efficiency all-inorganic full-colour quantum dot light-emitting diodes

Xuyong Yang^{a,*}, Zi-Hui Zhang^b, Tao Ding^c, Ning Wang^c, Guo Chen^a, Cuong Dang^c, Hilmi Volkan Demir^c, Xiao Wei Sun^{d,*}

^a Key Laboratory of Advanced Display and System Applications of Education of Ministry, Shanghai University, 149 Yanchang Road, Shanghai 200072, PR China

^b Institute of Micro-Nano Photoelectron and Electromagnetic Technology Innovation, School of Electronics and Information Engineering, Hebei University of Technology, 5340 Xiping Road, Beichen District, Tianjin 300401, PR China

^c Luminous! Center of Excellence for Semiconductor Lighting and Displays, School of Electrical and Electronic Engineering, School of Physical and Mathematical Sciences, Nanyang Technological University, Nanyang Avenue, Singapore 639798, Singapore

^d Department of Electrical and Electronic Engineering, Southern University of Science and Technology, 1088 Xue-Yuan Road, Shenzhen, Guangdong 518055, PR China

ARTICLE INFO

Keywords:

Electroluminescent devices
Quantum dots
Electroluminescence
Light-emitting diodes
Inorganic nanodevices

ABSTRACT

All-inorganic quantum dot light-emitting diodes (QLEDs) with excellent device stability have attracted significant attention for solid state lighting and flat panel display applications. However, the performance for the present all-inorganic QLEDs is far inferior to that of the well-developed QLEDs with organic charge transport layers. Our all-inorganic full-colour QLEDs show the maximum brightness and efficiency values of 21,600 cd/m² and 6.52%, respectively, which are record-breaking among the existing all-inorganic QLEDs. The outstanding performance is achieved by an efficient design of device architecture with solution-processed charge transport layers (CTLs). Meanwhile, the ultrathin double-sided insulating layers are inserted between the quantum dot emissive layer and their adjacent oxide electron transport layers to better balance charge injection in the device and reduce the quenching effects for inorganic CTLs on QD emission. This study is the first account for high-performance, all-inorganic QLEDs insightfully offering detailed investigations into the performance promotion for inorganic electroluminescent devices.

1. Introduction

Colloidal quantum dot (QD)-based light-emitting diodes (QLEDs) with advantages in narrow emission linewidth, tunable emission wavelength and cost-effectiveness are reaching organic LEDs' performance and emerging as a candidate for single material capable of full-colour light sources [1–8]. Currently, the most developed QLEDs employ organic semiconductors as the charge transport layers (CTLs). However, these organic layers are less stable compared with inorganic materials, especially under high current densities [9–11]. The stability of the present QLEDs has become a big concern for their practical applications in lighting and displays [12,13]. Despite their excellent device stability, the performance of inorganic QLEDs has been significantly lower than that of QLEDs with organic CTLs. The relatively poor device performance is mainly caused by the imbalanced carrier injection resulting from a large energy barrier between the metal-oxide CTL and the QDs as well as the strong quenching effect of the surrounding conductive metal oxide on the QD emission (charging QDs) [14–18].

To achieve high-performance all-inorganic QLEDs, it is therefore necessary to optimize the charge balance in devices and minimize the

negative influence of inorganic CTLs on QDs. The choice of charge transport materials for inorganic QLEDs is relatively limited compared to the well-developed organic molecules with excellent charge transport properties. Due to the better compatibility with QD deposition, solution-processed metal-oxide thin films with controllable morphologies and interface structures at the nanometer scale have been widely used as CTLs for QLEDs, which are more efficient than their bulk counterparts [19–24]. Till date, the reported highest efficiency values for all the red, green and blue (RGB) emitting QLEDs are based on the use of solution-processed ZnO nanoparticles (NPs) as the electron transport layer (ETL) [1,2,25]. Recently, the incorporation of an organic insulating thin layer between QDs and inorganic ZnO ETL has shown to improve the charge balance in QD layer, and by avoiding QD charging (ref. [1]), this design holds great promise for preserving excellent emissive properties of the QDs. This suggests the great potential that solution-processed multilayer structures with properly modulating charge injection could be used to improve the performance of all-inorganic QLEDs.

Here, we demonstrate high-performance all-inorganic QLEDs through an efficient device structure design where the solution-processed metal oxides served as charge transport layers. By inserting

* Corresponding authors.

E-mail addresses: yangxy@shu.edu.cn (X. Yang), sunxw@sustc.edu.cn (X.W. Sun).

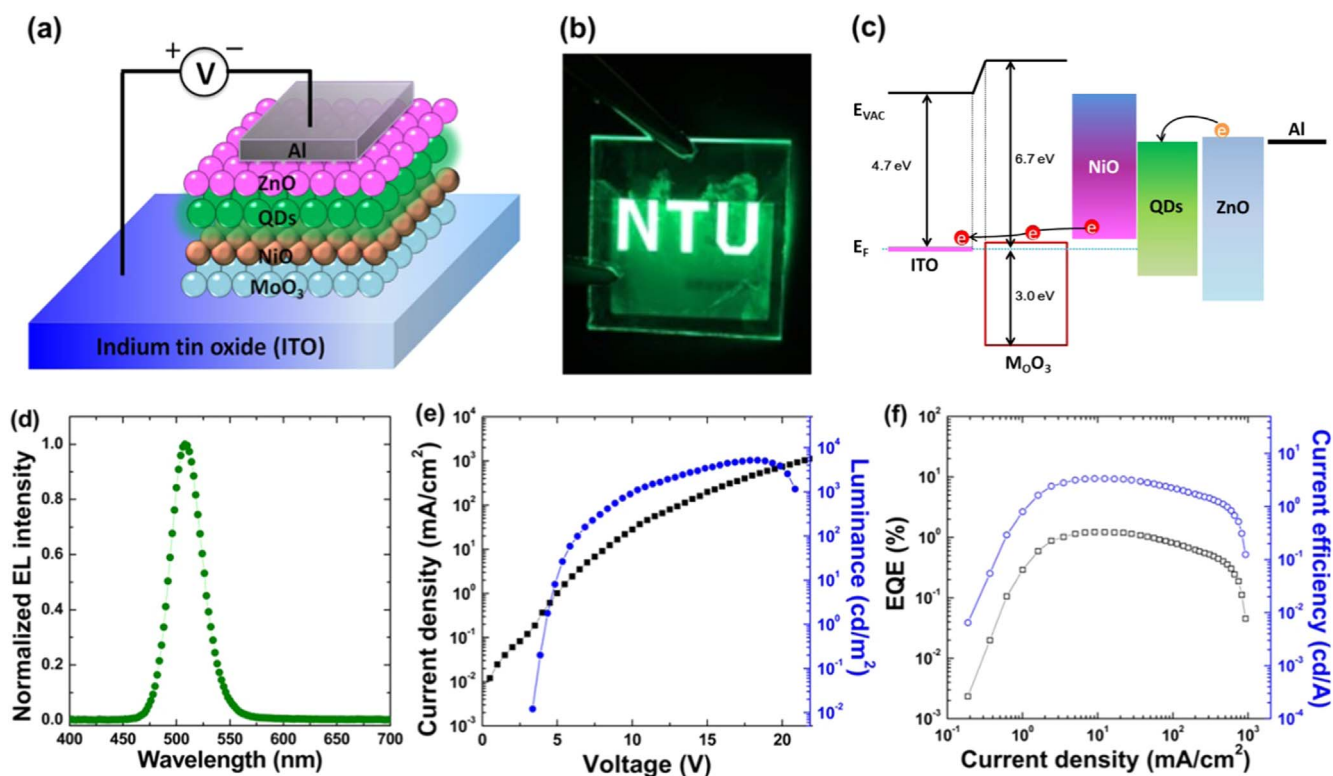


Fig. 1. (a) Schematic illustration of the QLED I with normal device architecture: ITO/MoO₃/NiO/QDs/ZnO/Al. (b) Photograph of a working device with the Nanyang Technological University logo. (c) Energy level diagram for the all-inorganic QLED devices. The energy levels for individual layers are taken from references [13,31–34]. (d) Normalized EL spectrum for the resultant QLED at an applied bias of 8 V. (e) Current density-voltage-luminance (*J-V-L*) characteristics. (f) Current efficiency and external quantum efficiency in terms of the current density.

insulating layers between the quantum dot layer and their adjacent solution-processed charge transport layers to adjust charge balance and to improve QD's emission efficiency, the performance of the resultant QLEDs is significantly improved and meanwhile the full-colour, all-inorganic QLEDs are achieved. The insulating thin layers inserted in QLEDs are designed here to be very thin, especially for the LiF layer deposited between QDs and NiO HTL which is a discontinuous nanosland layer, for avoiding the reduction of charge injection into QDs caused by the increase of system resistance. Our resultant QLEDs show the maximum luminance and EQE values of 21,600 cd/m² and 6.52%, respectively, which are the highest performance values for all-inorganic QLEDs ever reported up to date.

2. Experimental section

2.1. Synthesis of multicoloured QDs and ZnO nanoparticles

The red-emitting CdSe/Cds/ZnS core-double-shell QDs used in this work were prepared by a multiple injection method [26], and the yellow-, Green- and blue-emitting CdSe-ZnS QDs with core-shell alloyed structures were prepared by using a one-pot synthesis method [2,26]. The ZnO nanoparticles as ETL was prepared by a solution-precipitation method [23]. We mixed zinc acetate in dimethyl sulfoxide (DMSO) (0.1 M, 30 mL) and tetramethylammonium hydroxide in ethanol (0.5 M, 10 mL) and stirred the solution for 1 h in the ambient of dry air before, then precipitating the mixture with excess acetone. The as-prepared ZnO nanoparticles were dispersed in ethanol (~25 mg/mL).

2.2. Fabrication of QLED devices

We cleaned the substrates by sonication such that the ITO substrates were cleaned in detergent, DI-water, acetone, and isopropyl alcohol for 20 min, respectively. The ITO substrates were then treated by O₂-plasma

for 10 min and the diluted 2.5 wt% of MoO₃ xylene solution (purchased from Nanograde GmbH) was subsequently spin-coated on the substrate. The spinning rate was fixed at 6000 rpm for 60 s and then the coated film was annealed at 150 °C for 15 min to form the MoO₃ anode buffer layer [27]. The substrates were treated by O₂-plasma for removing polymeric dispersing agent and further functionalizing film. Next, the solution-processed NiO layer was deposited on the MoO₃ film from the coordination complex of MEA with Ni²⁺ (the mole ratio of Ni²⁺ to MEA is 1:1) by thermal decomposition at 4000 rpm for 60 s, which was then followed by annealing at 275 °C for 30 min [28]. The QD dispersion (QDs were dispersed in toluene with 15 mg/mL) was spin-coated on the ITO/MoO₃/NiO layer at a rate of 1000–4000 rpm for 60 s, and the QD dispersion was cured at 90 °C in the N₂ atmosphere for 30 min. After the QD layer, we dispersed the ZnO nanoparticles in ethanol, and the ZnO ETL was spin-coated on the ITO/MoO₃/NiO/QD architecture at a rate of 2000 rpm. The Al₂O₃ thin layer was prepared according to a previously reported method [29] and was spin-coated on QDs at a rate of 2000 rpm. Finally, the ultrathin LiF layer and Al cathode were deposited by thermal evaporation.

2.3. Measurements and characterizations

We measured the electroluminescence (EL) spectra for QLEDs by a Photo Research PR670 spectra scan spectrometer and the device performance measurement followed a technique described by Forrest et al. [30]. The surface morphologies for the spin-coated MoO₃, NiO, and ZnO NP layers were characterized by atomic force microscopy (Cypher AFM, Asylum Research). Transmission electron microscopy (TEM) images of quantum dots were obtained by using a transmission electron microscopy (JEOL, JEM-2010). Element mapping was performed using by energy-dispersive spectroscopy (EDS) on a field-emission scanning electron microscopy (FE-SEM). All the measurements were carried out at conditions of the room temperature and standard atmosphere.

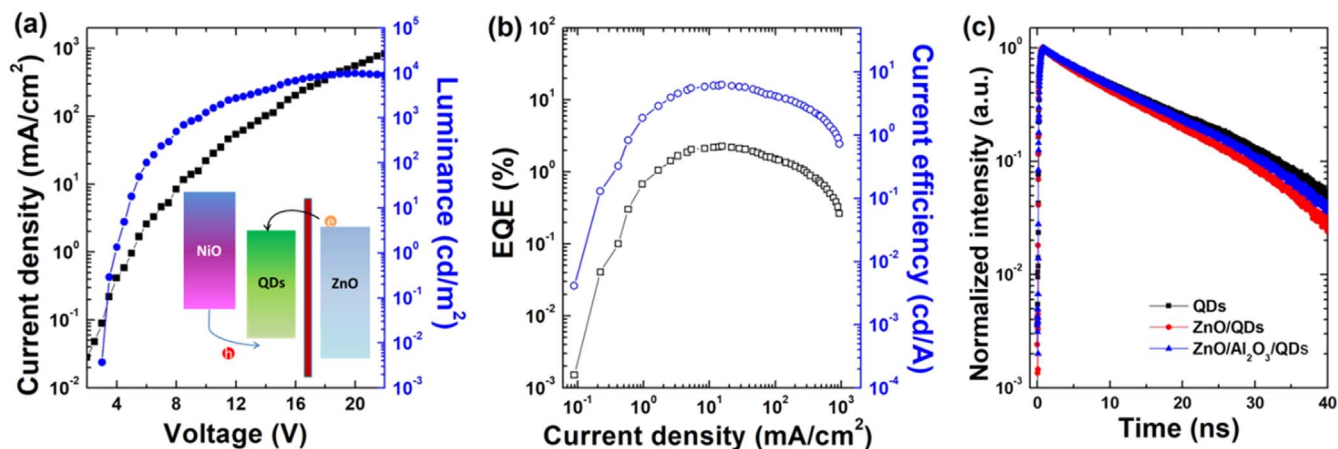


Fig. 2. (a) Current density and luminance of the QLED II as a function of applied bias. Inset shows the schematic diagram for the electron and hole injection into QD layer in QLED II. (b) EQE and CE of the QLED II as a function of current density. (c) Time-resolved fluorescence characteristics for QDs, ZnO/QDs and ZnO/Al₂O₃/QDs film.

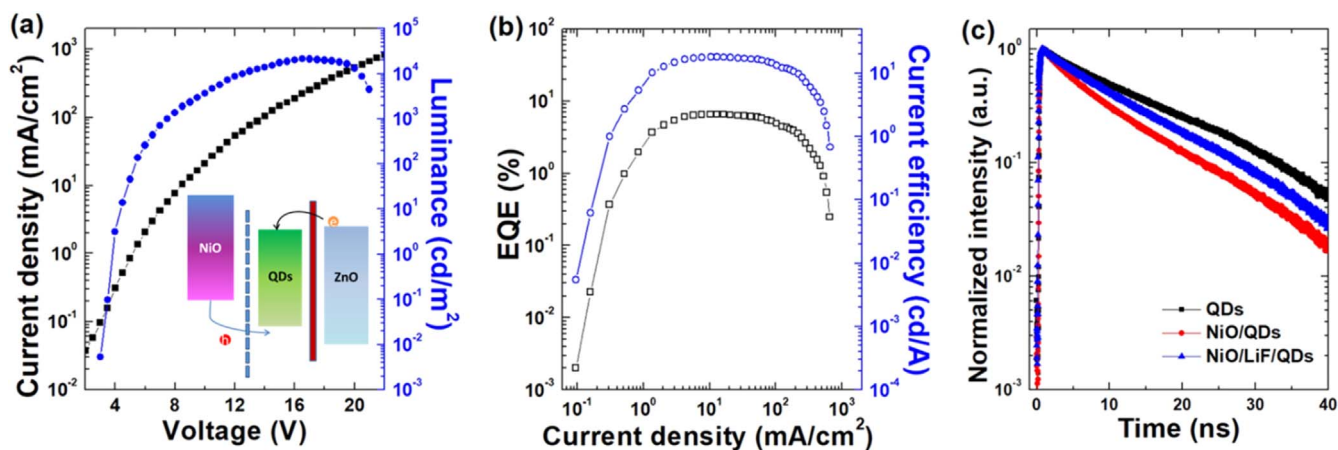


Fig. 3. (a) Current density and luminance for the QLED III as a function of the applied bias. Inset shows the schematic energy band diagram for the electron and hole injections into QD layer in QLED III. (b) EQE and CE for the QLED III as a function of the current density. (c) Time-resolved PL for QDs, NiO/QDs and NiO/LiF/QDs structures.

3. Results and discussion

Our all-inorganic QLEDs consist of multilayered thin film architectures of ITO/MoO₃/NiO/QDs/ZnO/Al, as shown in Fig. 1a. The core-shell structured CdSe/ZnS QDs with green emission are used for the emissive layer. The ZnO layer made from ZnO NPs in ethanol solution and NiO layer made from the coordination complex of monoethanolamine (MEA) with Ni by thermal decomposition were prepared as the ETL and the hole transport layer (HTL), respectively. The MoO₃ layer made from MoO₃ NPs xylene solution served as the hole injection layer (HIL). In the device architecture (QLED I), only the Al cathode was deposited by vacuum thermal evaporation and all the other layers were sequentially spin-coated onto the ITO layer. Fig. 1b presents a photograph for a working all-inorganic QLED, which displays uniform and bright green emission. From the corresponding schematic energy level diagram of the all-inorganic device (Fig. 1c), it can be observed that the electrons are injected from the Al cathode to the QD emissive layer via the conduction band of the ZnO layer while the hole injection from the ITO anode into the NiO layer results from electron breakthrough the MoO₃/NiO junction because of the deep lying electronic states of n-doped MoO₃ (the electrons are extracted from the valence band of NiO through the conduction band of MoO₃). It can be noted that the electrons in QLED I are much easier injected into QD layer compared with the hole injection because of the smaller energy barrier height between ZnO and QDs. Fig. 1d displays the electroluminescence (EL) spectrum of the resultant QLEDs. The peak wavelength of ~508 nm with a full width at half maximum (FWHM) of 35 nm emitted

by the QDs indicates the highly efficient radiative recombination between electrons and holes in the QD layer. We also show the current density and luminance in terms of the applied bias for the unpackaged QLEDs in Fig. 1e. The maximum luminance can reach 5200 cd/m² and the turn-on voltage (V_T) is as low as 3 V, suggesting that the efficient carrier injection into the QD emissive layer. The external quantum efficiency – current efficiency – current density (EQE - CE - J) characteristics for the inorganic QLED reveal the high device efficiency, such that a maximum EQE of 1.22% and CE of 3.4 cd/A are obtained according to Fig. 1f. These results indicate that the solution-processed metal-oxide thin films can serve as the excellent CTLs and offers a practical platform to realize low-cost, high-performance and robust QLEDs.

Charge-carrier dynamics in the QD emissive layer plays an important role in achieving high-performance QLEDs. The ZnO NPs as the currently most efficient ETL used in QLEDs often produces the excess electron current in a device due to the high electron mobility and small energy barrier between QDs and ZnO compared with hole transport materials, which leads to unbalanced charge in QLED devices. Also, metal-oxides usually quench the emission of QDs resulting from the ultrafast non-radiative process of inefficient trion emission that depends on the proximity of emitters to the interface [14]. To maximize the electrically driven QD emission from QLEDs, we inserted a thin Al₂O₃ film (~2 nm) between the ZnO layer and the QD layer to balance the carrier injection and avoid the charging of QD emissive layer (QLED II). Note that the electrons can be still efficiently injected into QD emissive layers by tunneling through the thin Al₂O₃ layer. With the incorporation of Al₂O₃ thin layer, the device performance is dramatically

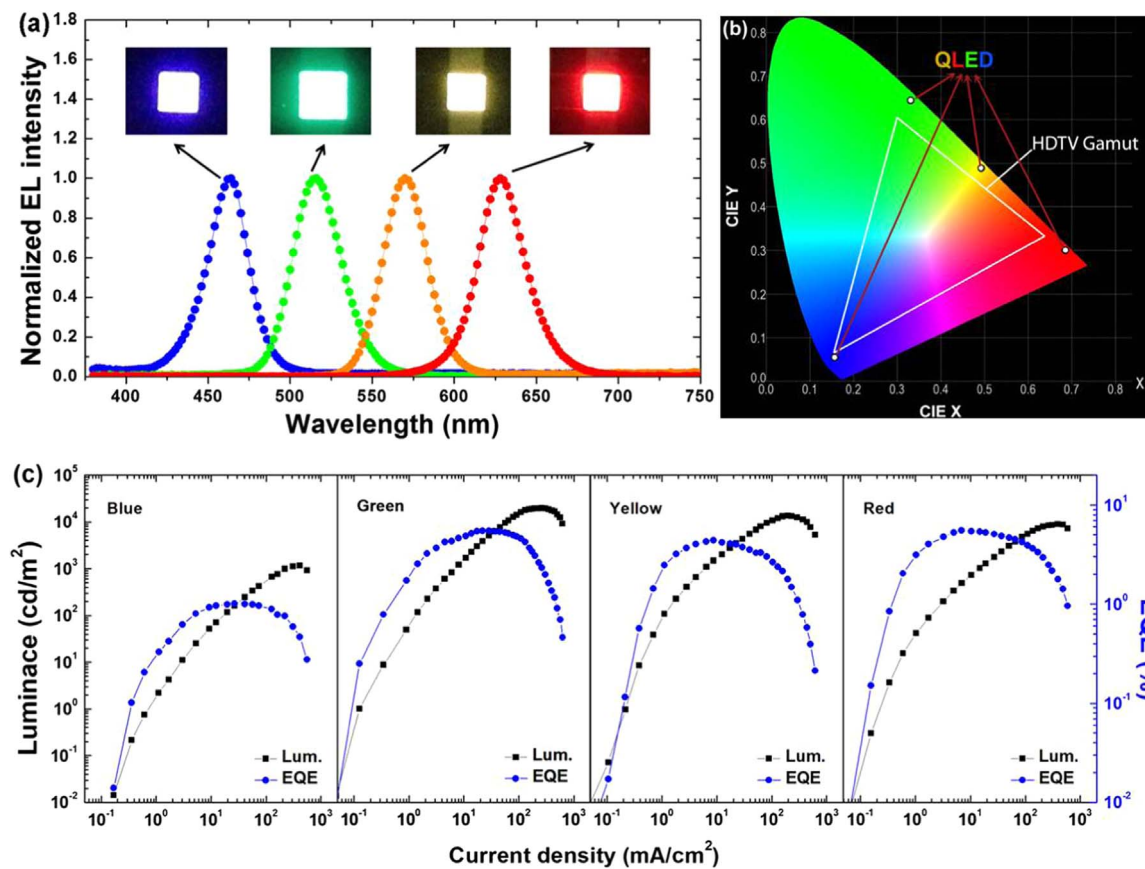


Fig. 4. (a) Normalized EL spectra for the all-inorganic QLEDs with the peak emission wavelengths of 464 nm (blue), 516 nm (green), 570 nm (yellow), and 630 nm (red). Inset: the corresponding images of the multi-colour QLEDs with a pixel size of 1 mm × 1 mm. (b) CIE coordinates for the four QLEDs together with the HDTV colour standards. (c) Luminance and EQE curves of our multi-colour devices as a function of the current density.

Table 1
Summary of the electrical properties of the multi-colour QLEDs.

Colour of QLED	EL λ_{max} (nm)	FWHM (nm)	V_T (V)	EQE _{max} (%)	L_{max} (cd/m ²)	CIE index (x, y)
Blue	464	29	5.5	1.01	1160	0.155, 0.058
Green (I)	508	35	3.0	6.52	21,630	0.121, 0.689
Green (II)	516	35	3.1	5.48	19,800	0.335, 0.631
Yellow	570	31	3.3	4.36	13,500	0.465, 0.492
Red	630	33	2.8	5.51	8870	0.679, 0.318

enhanced, as shown in Fig. 2a, the maximum luminance of QLED II reaches 9780 cd/m² at the applied bias of 17 V, 1.88 folds larger than that of the reference device (QLED I). It can be found that the current density of QLED II with the insertion of Al₂O₃ thin layer is slightly smaller than that of QLED I. Fig. 2b presents the EQE-CE-J curves that show a high CE of 6.3 cd/A at a luminance of 970 cd/m². This corresponds to an EQE level of 2.29%, significantly higher than that of QLED I (1.22%). The time-resolved photoluminescence (PL) spectroscopy is used to study the recombination processes within the QD emissive layer for the resultant QLED I and QLED II (Fig. 2c). The average PL lifetime of the QD films decreased from 13.81 to 11.64 ns after the deposition of the top ZnO NP films because of the inefficient negative trion emissions (a spontaneous charge transfer process will occur when the QDs are contact with the ZnO ETLs owing to their different work functions) [35]. However, the PL lifetime of QD film is increased to 13.03 ns after the insertion of Al₂O₃ thin film between QD and ZnO layers. These results indicate that the insertion of Al₂O₃ layer helps to maintain charge neutrality of the QD emissive layer and thus preserves the superior emissive properties of QDs, which are in good agreement with the previous findings [1].

In addition, we found that the QLED performance can be further improved when an ultrathin LiF “nanoisland” layer is inserted between QDs and NiO layer (QLED III). As shown in Fig. 3a, the maximum luminance reaches 21,630 cd/m² at an applied bias of 16.5 V when a LiF thin layer of ~0.3 nm is deposited between QDs and NiO layer, with the maximum EQE of 6.52% and CE of 17.8 cd/A (Fig. 3b). The insertion of double-sided inorganic insulating layers improves the efficiency and brightness of our all-inorganic QLEDs by 170% and 133% compared with QLED II, respectively. The resulting all-inorganic QLEDs show a long device lifetime of 16, 120 h at 100 cd/m² (Supplementary Fig. S1). It worth pointing out that the insertion of LiF insulating layer between QDs and NiO layer will decrease the hole injection into QD layer because of the huge energy barrier from NiO to LiF. Therefore, the reasons for the performance enhancement can be primarily attributed to that the insertion of the LiF nanoisland layer avoids the charging of QDs. This is further confirmed by the dramatic lifetime increase of the quantum dot film from 7.7 ns to 11.2 ns when the LiF thin layer is inserted between QDs and NiO layer (Fig. 3c). Meanwhile, the thickness of LiF layer should be very thin to reduce the hole blocking effect of LiF layer to the minimum. In our case the LiF layer deposited on the NiO

HTL is only ~ 0.3 nm, which is not a continuous thin film. Instead, the LiF nanoislands on the NiO surface can be expected (Supplementary Fig. S2). In other words, the LiF layer on the NiO behaves as a huge valance band barrier and reduces hole injection efficiency, however, the LiF exists as the nanoislands, and therefore, the holes can be efficiently injected into the QD regions through the more conductive NiO channels embedded among the LiF nanoislands. As a result, there is no dramatic effect on the hole injection when the LiF is deposited on the NiO surface.

Using our optimized device structures with multi-colour QDs, we further tested the full-colour, all-inorganic QLEDs. The EL spectra for these all-inorganic QLEDs with four different emission wavelengths (464, 516, 570, and 630 nm) at the applied bias of 8 V are shown in Fig. 4a. We can see that all the EL spectra are saturated with the narrow-linewidth emission of QDs and the FWHM is 29, 35, 31 and 33 nm for the respective colour. The inset presents the corresponding photographs for the four operating QLED devices, which displays nearly saturated colour emission. As presented by the Commission Internationale de Eclairage (CIE) chromaticity diagram (Fig. 4b), the coverage area for these fabricated QLEDs is larger than the standard colour triangle area of the high-definition television (HDTV) [12,36]. The luminance and EQE as a function of the current density for the resultant multi-colour QLEDs are shown in Fig. 4c. Very high performances for all the devices were achieved and summarized in Table 1 (the transmission electron microscopy (TEM) images of these QDs are shown in Supplementary Fig. S3). Although the record luminance and efficiency values are reported in this work for the correspondingly coloured all-inorganic QLEDs, we still expect the even better device performances by e.g., improving the quantum yields for QD films and/or using solution-processed insulating layers.

4. Conclusion

In conclusion, we have demonstrated full-colour, all-inorganic QLEDs with record high electroluminescence efficiency and peak luminance values. The superior performance was achieved by the use of solution-processed metal-oxide films compatible with QDs deposition and the efficient design of device architecture with the insertion of double-sided insulating thin layers between QDs and their adjacent charge transport layers. These findings suggest that the interfacial engineering is quite critical for improving the performance of QLEDs and our approach may have important implications for designing high-efficiency inorganic QLEDs and understanding device physics by optimizing charge balance and modifying interface properties.

Acknowledgements

The authors would like to thank the financial support from National Key Research and Development Program of China administered by the Ministry of Science and Technology of China (No. 2016YFB0401702), National Natural Science Foundation of China (Nos. 51675322, 61605109, 61735004 and 61674074), Shenzhen Peacock Team Project (No. KQTD2016030111203005), Shenzhen Innovation Project (No. JCYJ20160301113356947, JCYJ20150630145302223 and JCYJ20160301113537474). X. Yang also thanks the Program for Professor of Special Appointment (Eastern Scholar) at Shanghai Institutions of Higher Learning (No. TP2015037).

Appendix A. Supporting information

Supplementary data associated with this article can be found in the online version at <http://dx.doi.org/10.1016/j.nanoen.2018.02.002>.

References

- [1] X. Dai, Z. Zhang, Y. Jin, Y. Niu, H. Cao, X. Liang, L. Chen, J. Wang, X. Peng, *Nature* 515 (2014) 96–99.
- [2] Y. Yang, Y. Zheng, W. Cao, A. Titov, J. Hyvonen, J.R. Manders, J. Xue, P.H. Holloway, L. Qian, *Nat. Photon.* 9 (2015) 259–266.
- [3] B.S. Mashford, M. Stevenson, Z. Popovic, C. Hamilton, Z. Zhou, C. Breen, J. Steckel, V. Bulovic, M. Bawendi, S. Coe-Sullivan, P.T. Kazlas, *Nat. Photon.* 7 (2013) 407–412.
- [4] J. Kwak, W.K. Bae, D. Lee, I. Park, J. Lim, M. Park, H. Cho, H. Woo, D.Y. Yoon, K. Char, S. Lee, C. Lee, *Nano Lett.* 12 (2012) 2362–2366.
- [5] X. Yang, D. Zhao, K.S. Leck, S.T. Tan, Y.X. Tang, J. Zhao, H.V. Demir, X.W. Sun, *Adv. Mater.* 24 (2012) 4180–4185.
- [6] Y. Zou, M. Bang, W. Cui, Q. Huang, C. Wu, J. Liu, H. Wu, T. Song, B. Sun, *Adv. Funct. Mater.* 27 (2017) 1603325.
- [7] B.H. Kim, S. Nam, N. Oh, S.-Y. Cho, K.J. Yu, C.H. Lee, J. Zhang, K. Deshpande, P. Trefonas, J.-H. Kim, J. Lee, J.H. Shin, Y. Yu, J.B. Lim, S.M. Won, Y.K. Cho, N.H. Kim, K.J. Seo, H. Lee, T. Kim, M. Shim, J.A. Rogers, *ACS Nano* 10 (2016) 4920–4925.
- [8] Y.-H. Kim, G.-H. Lee, Y.-T. Kim, C. Wolf, H.J. Yun, W. Kwon, C.G. Park, T.-W. Lee, *Nano Energy* 38 (2017) 51–58.
- [9] M. Tian, J. Luo, X. Liu, *Opt. Express* 17 (2009) 21370–21375.
- [10] H. Zhang, N. Sui, X. Chi, Y. Wang, Q. Liu, H. Zhang, W. Ji, *ACS Appl. Mater. Interfaces* 8 (2016) 31385–31391.
- [11] W. Ji, S. Liu, H. Zhang, R. Wang, W. Xie, H. Zhang, *ACS Photonics* 4 (2017) 1271–1278.
- [12] Y. Shirasaki, G.J. Supran, M.G. Bawendi, V. Bulović, *Nat. Photon.* 7 (2013) 13–23.
- [13] F. Cao, H. Wang, P. Shen, X. Li, Y. Zheng, J. Zhang, Y. Shang, Z. Ning, X. Yang, *Adv. Funct. Mater.* 27 (2017) 1704278.
- [14] J.M. Caruge, J.E. Halpert, V. Wood, V. Bulovic, M.G. Bawendi, *Nat. Photon.* 2 (2008) 247–250.
- [15] V. Wood, M.J. Panzer, J.E. Halpert, J.-M. Caruge, M.G. Bawendi, V. Bulovic, *ACS Nano* 3 (2009) 3581–3586.
- [16] V. Wood, V. Bulović, *Nano Rev.* 1 (2010) 5202–5208.
- [17] W. Qin, H. Liu, P. Guyot-Sionnest, *ACS Nano* 8 (2014) 283–291.
- [18] D. Bozyigit, O. Yarema, V. Wood, *Adv. Funct. Mater.* 23 (2013) 3024–3029.
- [19] L. Qian, Y. Zheng, J. Xue, P.H. Holloway, *Nat. Photon.* 5 (2011) 543–548.
- [20] K.-S. Cho, E.K. Lee, W.-J. Joo, E. Jang, T.-H. Kim, S.J. Lee, S.-J. Kwon, J.Y. Han, B.-K. Kim, B.L. Choi, J.M. Kim, *Nat. Photon.* 3 (2009) 341–345.
- [21] X. Yang, E. Mutlugun, Y. Zhao, Y. Gao, K.S. Leck, Y. Ma, L. Ke, S.T. Tan, H.V. Demir, X.W. Sun, *Small* 10 (2014) 247–252.
- [22] T. Ding, X. Yang, L. Bai, Y. Zhao, K.E. Fong, N. Wang, H.V. Demir, X.W. Sun, *Org. Electron.* 26 (2015) 245–250.
- [23] K.-H. Lee, J.-H. Lee, W.-S. Song, H. Ko, C. Lee, J.-H. Lee, H. Yang, *ACS Nano* 7 (2013) 7295–7302.
- [24] K.-H. Lee, J.-H. Lee, H.-D. Kang, B. Park, Y. Kwon, H. Ko, C. Lee, J. Lee, H. Yang, *ACS Nano* 8 (2014) 4893–4901.
- [25] H. Shen, W. Cao, N.T. Shewmon, C. Yang, L.S. Li, J. Xue, *Nano Lett.* 15 (2015) 1211–1216.
- [26] W.K. Bae, J. Kwak, J. Lim, D. Lee, M.K. Nam, K. Char, C. Lee, S. Lee, *Nano Lett.* 10 (2010) 2368–2373.
- [27] J. Meyer, R. Khalandovsky, P. Görrn, A. Kahn, *Adv. Mater.* 23 (2011) 70–73.
- [28] J.R. Manders, S.-W. Tsang, M.J. Hartel, T.-H. Lai, S. Chen, C.M. Amb, J.R. Reynolds, F. So, *Adv. Funct. Mater.* 23 (2013) 2993–3001.
- [29] J. Peng, Q. Sun, Z. Zhai, J. Yuan, X. Huang, Z. Jin, K. Li, S. Wang, H. Wang, W. Ma, *Nanotechnology* 24 (2013) 484010.
- [30] S.R. Forrest, D.D.C. Bradley, M.E. Thompson, *Adv. Mater.* 15 (2003) 1043–1048.
- [31] Z. Xiao, R.A. Kerner, L. Zhao, N.L. Tran, K.M. Lee, T.-W. Koh, G.D. Scholes, B.P. Rand, *Nat. Photon.* 11 (2017) 108–115.
- [32] M. Kröger, S. Hamwi, J. Meyer, T. Riedl, W. Kowalsky, A. Kahn, *Appl. Phys. Lett.* 95 (2009) 123301.
- [33] T. Ding, N. Wang, C. Wang, X. Wu, W. Liu, Q. Zhang, W. Fan, Xiao Wei Sun, *RSC Adv.* 7 (2017) 26322–26327.
- [34] X. Yang, Y. Ma, E. Mutlugun, Y. Zhao, K.S. Leck, S.T. Tan, H.V. Demir, Q. Zhang, H. Du, X.W. Sun, *ACS Appl. Mater. Interfaces* 6 (2014) 495–499.
- [35] W.K. Bae, Y.-S. Park, J. Lim, D. Lee, L.A. Padilha, H. McDaniel, I. Robel, C. Lee, J.M. Pietryga, V.I. Klimov, *Nat. Commun.* 4 (2013) 2661.
- [36] X. Yang, E. Mutlugun, C. Dang, K. Dev, Y. Gao, S.T. Tan, X.W. Sun, H.V. Demir, *ACS Nano* 8 (2014) 8224–8231.